J Appl Electrochem (2013) 43:659–666
DOI 10.1007/s10800-013-0557-y

ORIGINAL PAPER

Oxidative dissolution of pyrite in acidic media

Cristina A. Constantin · Paul Chiriţă

Received: 9 March 2013 / Accepted: 3 May 2013 / Published online: 31 May 2013

Abstract The pyrite oxidative dissolution in air-saturated (AS), H_2O_2, and Fe^{3+} solutions at pH 2.5 and 25 °C was investigated by electrochemical and aqueous batch experiments. The corrosion current density (i_{corr}) increases from AS solution to Fe^{3+} and H_2O_2 solutions. For the same oxidant, i_{corr} increases when the concentration of the oxidant increases. Similar variation was observed for the corrosion potential (E_{corr}). Electrochemical impedance spectroscopy measurements have indicated that in AS and H_2O_2 solutions, the charge transfer is the rate determining step of pyrite oxidative dissolution. In the presence of $Fe^{3+}_{(aq)}$, both the charge transfer process and mass transfer caused by the diffusion of oxidant or reaction products across the interface of electrode control the mineral oxidative dissolution. The corrosion current densities of oxidative dissolution measured by electrochemical methods are higher than those estimated from dissolution rates determined by aqueous bath experiments. The observed differences suggest that the mechanism of polarized electrode oxidation is different by the mechanism of pyrite oxidation under open circuit conditions.

Keywords Pyrite · Oxidation · Mechanism · Electrochemical impedance spectroscopy

1 Introduction

Pyrite is the most abundant terrestrial mineral sulfide, and it is usually associated with other sulfides, coal beds, and uranium ores [1]. The aqueous oxidation of pyrite is a reaction involved in various natural and industrial processes like ore processing, metal extraction, and acid mine drainage (AMD) formation. Therefore, a large number of studies have been carried out in order to understand the reaction products and mechanism of pyrite oxidation [1–7].

The reaction products of pyrite oxidation were studied by various techniques including aqueous batch and electrochemical experiments and spectroscopic analysis. Descostes et al. [7] detected only Fe^{2+} and SO_4^{2-} in the oxidant solutions [25 °C, pH < 3 and air-saturated (AS) suspensions]. Moreover, they reported a deficit in aqueous sulfur with respect to dissolved iron. The presence of a sulfur rich (or metal deficient) layer on reacted pyrite in Fe^{3+} solutions at low pH was found by Sasaki et al. [8] and Giannetti et al. [5]. Wei and Osseo-Asare [9] have found the elemental sulfur (S^0) among the anodic dissolution products of pyrite in acidic media. The most accepted origin of elemental sulfur on mineral surface is the disproportionation of $S_2O_3^{2-}$ (resulted from pyrite oxidation) into S^0 and HSO_3^-, but not direct oxidation of pyrite to S^0 [10].

Williamson and Rimstidt [11] observed that the rates of interaction between pyrite and aqueous oxidants strongly correlate with Eh. They concluded that pyrite oxidation occurs after an electrochemical mechanism. Instead, Wei and Osseo-Asare [9] found that in acidic solution, pyrite dissolution shows both electrochemical and chemical features. The authors underlined the essential role played by water in pyrite dissolution, that is, generator of hydroxyl groups that intermediate the electrochemical reaction (the oxidation of surface S_2^{2-} groups) and H^+ and/or HO^- that enables the chemical reaction (the breaking of Fe–S bounds). There are also doubts about the nature of the oxidant. It is believed that at low pH values, the pyrite

C. A. Constantin · P. Chiriţă (✉)
Department of Chemistry, University of Craiova, Calea Bucuresti, 107I, 200512 Craiova, Romania
e-mail: paulxchirita@gmail.com

oxidant is ferric iron (Fe^{3+}) rather than dissolved oxygen. Because of the low solubility of Fe^{3+} at higher pH values, it is assumed that dissolved oxygen ($O_{2(aq)}$) is the oxidant [2].

In this paper, the oxidative dissolution of pyrite was studied in different oxidant media by both aqueous batch and electrochemical [polarization measurements and electrochemical impedance spectroscopy (EIS)] experiments. For a better understanding of mineral oxidation mechanism, we planned to compare the results of electrochemical experiments with those of aqueous batch experiments, both performed in the presence of the main oxidants of pyrite: $O_{2(aq)}$, $H_2O_{2(aq)}$, and $Fe^{3+}_{(aq)}$. The most relevant comparison was made between the corrosion current densities derived from oxidation rates obtained in course of aqueous batch experiments and, respectively, measured during the electrochemical experiments. Also the initial and reacted pyrite samples were investigated by FTIR spectroscopy.

2 Experimental

2.1 Materials

The mineral used in this study was identified by X-ray diffraction as pyrite. No other phases could be detected. The content of trace impurities (Co, Ni, Cu, Zn, and As) was below 0.2 % (mass percentage) [12, 13]. Hydrogen peroxide, ferric chloride, and hydrochloric acid used in the experiments were of reagent grade purity. The solutions of H_2O_2 and Fe^{3+} were prepared with distilled water deaerated by boiling. The saturation with oxygen was accomplished by bubbling air through acidic solutions for at least 1 h. Before each experiment, pH was set to 2.5. The pH of the solutions was measured at experimental temperature (25 °C) with a combined glass electrode (Consort), calibrated against two pH buffers (pH 4.01 and pH 7.00).

2.2 Electrochemical experiments

A classical three-electrode glass cell was used for electrochemical experiments. The working electrode was made of pyrite. The pyrite sample was cut into cubic shape and one side of cube was rooted to a Cu wire with C conductive glue. The cube was embedded in epoxy resin and cut to expose a mineral surface of 1 cm^2. Before each experiment, the electrode surface was polished by 600 and 3000 SiC paper, immersed in HNO_3 1 M for 1 min, rinsed several times with distilled water, and finally dried with acetone. The counter electrode was a platinum foil and the reference electrode was a saturated calomel electrode (SCE) ($E = 0.2415$ V vs. SHE). Electrochemical measurements were performed using an electrochemical workstation ZAHNER Elektrik IM6e controlled by Thales software. Before each experiment, the electrode was equilibrated for no less than 10 min to assure steady states. The polarization curves were recorded at a scanning rate of 1 mV/s and in range −0.25 to 0.25 V versus open circuit potential (OCP). The obtained polarization data were analyzed by Thales software in order to obtain corrosion potential (E_{corr}) and corrosion current densities (i_{corr}). Electrochemical impedance spectroscopy (EIS) was performed at OCP, in the frequency range of 10 mHz–3 MHz and with AC amplitude of 10 mV.

2.3 Dissolution experiments

Pyrite pieces were ground and sieved, and particle fraction 90–125 μm was selected for dissolution experiments. The geometric surface area (A_{geo}) of this fraction was evaluated according to the method proposed by Liu et al. [14]. The obtained value was 0.0113 m^2/g. The pyrite grains were treated with a solution of 1 M HNO_3 in order to remove the fine particles and oxides existing on the surface [1]. Aqueous batch experiments were performed by adding 0.4 g pyrite to 250 mL oxidant solutions at pH 2.5 and 25 °C. The dissolution reaction was followed by monitoring the concentration of released sulfate. For sulfate analysis, 20 mL solution was withdrawn from the reactor with a syringe connected to a 0.4-μm filter. The released sulfate was determined by turbidimetric method at 420 nm [15]. In order to test the presence of aqueous species containing sulfur in low and intermediate oxidation states (like S_2^{2-}, $S_2O_3^{2-}$, SO_3^{2-}, or $S_4O_6^{2-}$), from the final solutions a separate sample of 20 mL was analyzed for sulfate after the addition of bromine water [16]. Bromine water oxidizes the aqueous species containing sulfur in low or intermediate oxidation states to SO_4^{2-} [16]. Because there were no registered meaningful differences between the determined [SO_4^{2-}], we can conclude that all the amount of dissolved sulfur is in the form of SO_4^{2-}.

At the end of the dissolution experiments, the reacted FeS_2 grains were separated from aqueous solutions, rinsed with distilled water, dried and stored in an evacuated desiccator until analyzed by FTIR spectroscopy.

2.4 FTIR measurements

The FTIR spectra were recorded with a Bruker Alpha spectrometer. KBr pellets containing the initial and reacted pyrite samples were used for the analysis. FTIR measurements were preformed in 400–4000 cm^{-1} range with a resolution of 4 cm^{-1}. Reference spectra of pyrite and its representative oxidation products were taken from the literature [17–20].

3 Results and discussion

3.1 Polarization measurements

Figure 1 shows the anodic and cathodic curves recorded for pyrite immersed in different oxidant solutions at pH 2.5. The shapes of both anodic and cathodic curves presented in Fig. 1a are quite similar. In contrary, the anodic and cathodic curves registered at high concentrations of H_2O_2 and Fe^{3+} have different shapes (Fig. 1b). The anodic curve of the experiment performed in the presence of ferric iron ($[Fe^{3+}]$=0.01 M) shows a small inhibiting plateau in the potential range 0.75–0.85 V. Most probably, this inhibiting plateau is due to the thick layer of elemental sulfur (or metal-deficient sulfide) formed on the mineral surface [6], whose development is favored by the high concentration of Fe^{3+}, an effective oxidant [8]. It is further oxidized to higher oxidation states. The corrosion kinetic parameters derived from these curves are presented in Table 1. The lowest corrosion current density (i_{corr}) was recorded in the case of AS solution [where the oxidant is $O_{2(aq)}$]. It increases for $Fe^{3+}_{(aq)}$ and $H_2O_{2(aq)}$. For the same oxidant, i_{corr} increases when the concentration of the oxidant increases. Since the slope of anodic curve is not well defined, i_{corr} value for the experiment carried out in solution with $[Fe^{3+}]$=0.01 M was obtained by the extrapolation of cathodic Tafel slope to the OCP (i.e., E_{corr} from Table 1). Similar trends were observed for the corrosion potential (E_{corr}). The highest corrosion potential was recorded in the presence of H_2O_2 solution with 0.1 M concentration. The lowest potential was observed in the case of pyrite immersed in AS solution. From Table 1, we can observe that the anodic Tafel slopes (ba) vary less, indicating that mechanism of electron transfer from pyrite is not dependent on nature and concentration of the acceptor of electrons. Only ba registered in the case of the experiment performed in 0.1 M H_2O_2 were almost twice as much as that recorded in the other experiments. This behavior could be explained by the oxygen produced by H_2O_2 decomposition [12, 13], which is adsorbed onto the surface of electrode and alter the mechanism of electron transfer from pyrite. It should be noted that the anodic Tafel slope for the experiment of pyrite immersed in 0.01 M Fe^{3+} was not determined. Instead, the cathodic Tafel slopes (bc) largely vary, indicating that the mechanism of electron acceptance (and implicitly overall oxidative dissolution of pyrite) is a function of the nature and concentration of the oxidant.

3.2 Electrochemical impedance spectroscopy (EIS)

EIS measurements were recorded in AS, H_2O_2, or Fe^{3+} solutions. The impedance diagrams recorded in AS and 0.001 M H_2O_2 solutions are shown in Fig. 2 in the form of

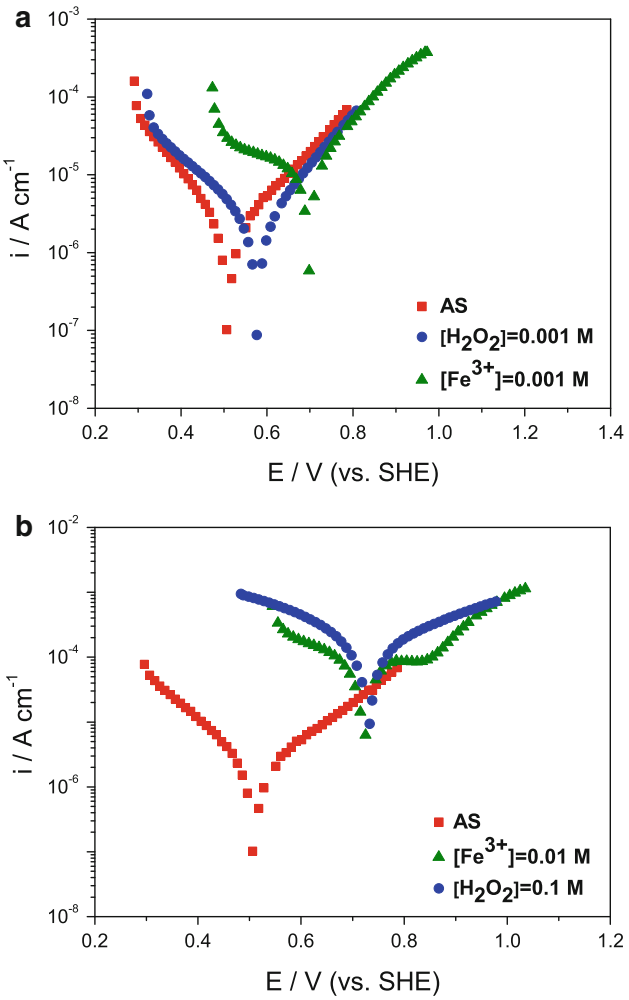

Fig. 1 Polarization curves for pyrite in AS, H_2O_2, and Fe^{3+} solutions at pH 2.5

Nyquist plots. In Fig. 3 is presented the Nyquist plot of pyrite immersed in 0.1 M H_2O_2 solution. The results of the experiments performed in the presence of dissolved ferric iron ($[Fe^{3+}]$=0.001 M and $[Fe^{3+}]$=0.01 M) are presented in Fig. 4. In Figs. 2, 3, and 4 are also presented the equivalent circuits used to fit the experimental data. EIS data presented in a figure were fitted by the same circuit, which differs from those presented in the other figures. This fact suggests different electrochemical mechanisms of pyrite interaction with oxidant solutions. The equivalent circuits shown in Figs. 2, 3, and 4 were selected to give the best fit with the experimental data. In literature, there are situations when the interaction of a particular mineral with aqueous solutions is modeled by different equivalent circuits (see the case of pyrite [21–23] or chalcopyrite [21, 24]). Therefore, finding the best equivalent circuit is often a laborious process. Our strategy to find the best equivalent circuits was the following. We started testing with the models proposed by Liu et al. [22]. When was appropriate,

Table 1 Polarization parameters for pyrite in HCl solutions (pH 2.5) containing O_2, H_2O_2, and Fe^{3+}

Oxidant	Concentration/M	i_{corr}/μA cm^{-2}	E_{corr}/mV	ba/mV dec^{-1}	bc/mV dec^{-1}
$O_{2(aq)}$	Saturated	1.78	514.4	177	−149
$H_2O_{2(aq)}$	0.001	2.19	585.6	147	−207
	0.1	143.00	749.7	304	−308
$Fe^{3+}_{(aq)}$	0.001	10.70	700.7	150	−514
	0.01	32.16	723.2	–	−267

to increase the quality of fitting, at these circuits, we have carefully added new elements chosen from theoretical considerations. Thus, the final equivalent circuits provide the best fittings and are consistent with the general mechanism of interaction of pyrite with oxidizing solutions. It should be noted that beside the circuits in Figs. 2, 3, and 4, we tested also the models proposed by Velasquez et al. [21] and Lehner et al. [23], but the results showed that our proposed models provided the best fitting.

In circuits from Figs. 2, 3, and 4, R_s is the ohmic resistance of the solution. It was experimentally measured, and the equivalent circuits were constrained with the corresponding values [23]. R_{pl} is the resistive component of the mass transport across the reaction product(s) layer developed on pyrite surface. C_{pl} is the capacitance exerted by this layer, that is, the capacitance of the capacitor consisting of the pyrite and the electrolyte with the product layer as dielectric. R_{ct} is the charge transfer resistance, and Q_{dl} is the double-layer capacitance. W is a Warburg element which takes into consideration diffusion effects. The use of this circuit element was suggested by the line situated in the region of low frequencies of the electrochemical impedance spectra registered in the presence of ferric iron solutions. The line forms an angle nearly 45° with the real impedance axis (Z'). It should be mentioned that because the impedance loops corresponding to the double layer recorded during our experiments are depressed to some extent but not ideal semicircles, the capacitors were substituted with constant phase elements (CPE) in order to produce more accurate fitting results. CPE is an element whose impedance is defined as:

$$Z_{CPE} = \frac{1}{Q \times (j\omega)^n} \quad (1)$$

where Q is magnitude of CPE, ω is the angular frequency at which imaginary impedance is maximum, $j^2 = -1$, and n is CPE exponent.

The semicircles registered at high frequencies in AS and 0.001 M H_2O_2 solutions are magnified and presented in

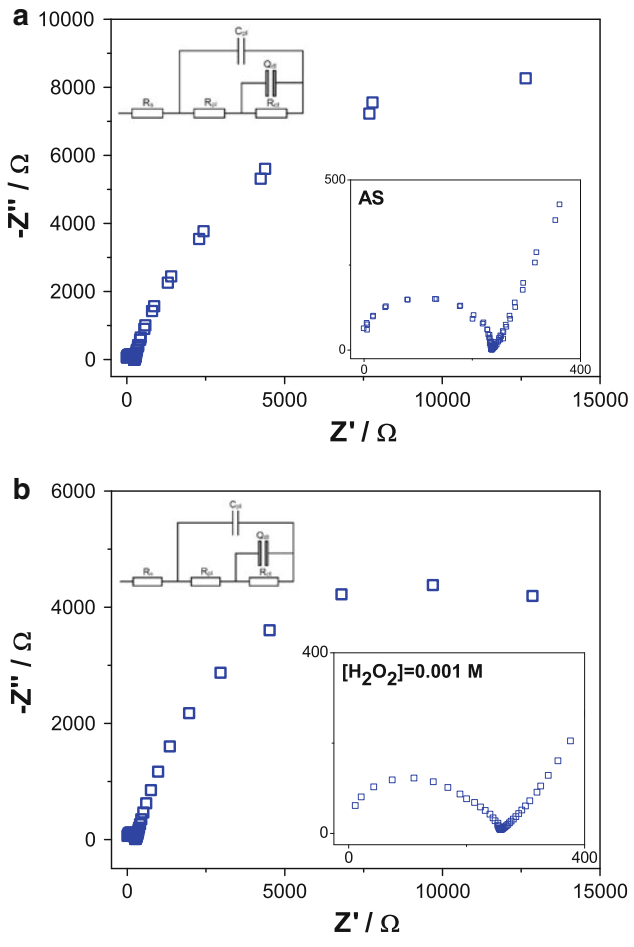

Fig. 2 Nyquist plot for pyrite in AS (**a**) and 0.001 M H_2O_2 (**b**) solutions. Best fitting results were obtained with the equivalent circuit presented in each plot

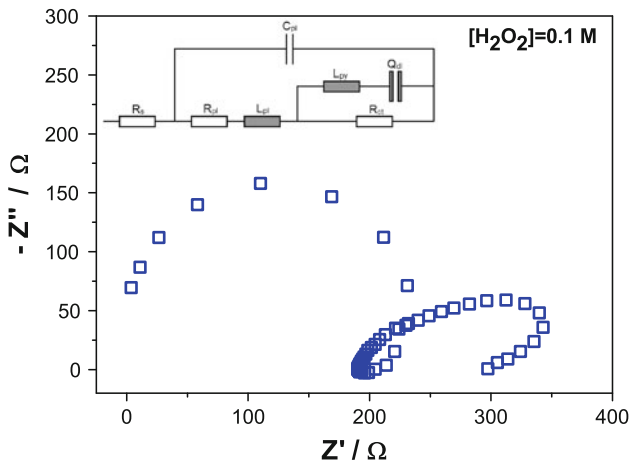

Fig. 3 Nyquist plot for pyrite immersed in 0.1 M H_2O_2 solution and the fitting circuit

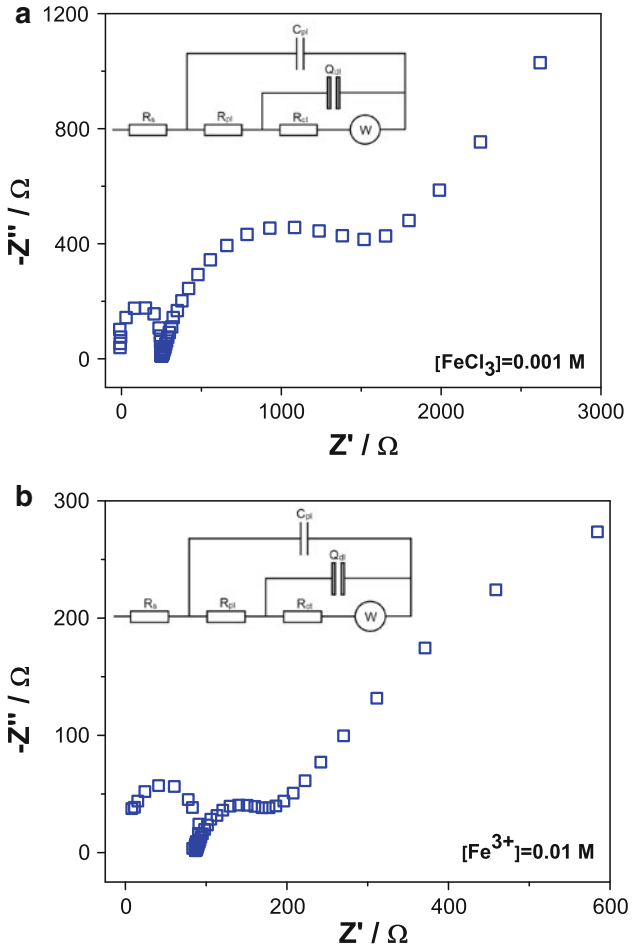

Fig. 4 Nyquist plot for pyrite immersed in 0.001 M (**a**) and 0.01 M (**b**) Fe^{3+} solutions. Best fitting results were obtained with the equivalent circuit presented in each plot

small windows within the Nyquist plots (Fig. 2). In the case of the solution with $[H_2O_2] = 0.1$ M, the equivalent circuit from Fig. 2 was completed by two inductances L_{pl} and L_{py}. These inductances can be correlated with middle and low frequencies adsorption processes of oxygen (resulted from H_2O_2 decomposition) on pyrite (L_{py}) and product(s) layer (L_{pl}). Fitting results are listed in Table 2. It is worth to note that R_{pl} values are close, while R_{ct} broadly decreases when E_{corr} increases. Hence, it is reasonable to consider that the semicircle found at low frequencies is caused by the charge transfer process, characterized by the charge transfer resistance (R_{ct}). From Table 2, it is easy to observe that $C_{pl} \ll Q_{dl}$. This relationship suggests that product(s) layer has a small thickness. n_{dl} was higher than 0.5 and indicates that the corresponding CPE behaves more as a capacitance.

In conclusion, EIS results indicate that in AS and H_2O_2 solutions, the charge transfer process controls the rate of mineral oxidation. In the presence of $Fe^{3+}_{(aq)}$, the dissolution rate is controlled by both charge transfer process and mass transfer caused by the diffusion of oxidant or reaction products across the interface of electrode.

3.3 Dissolution experiments

In order to better understand the mechanism of aqueous oxidation of pyrite, the mineral oxidative dissolution in the presence of AS, H_2O_2, and Fe^{3+} solutions was investigated by monitoring the concentration of released sulfate [(SO_4^{2-})]. Variation in [SO_4^{2-}] as a function of time at 25 °C and in the presence of above-mentioned oxidants is plotted in Fig. 5.

The fastest increase in [SO_4^{2-}] was observed in the experiment performed in 0.01 M $Fe^{3+}_{(aq)}$. [SO_4^{2-}] increases from 0 to 25.6 μM after 240 min. The slowest increase in [SO_4^{2-}] was registered in the case of AS solution. The values presented in Fig. 5a are average of the values obtained in three different experiments. The determined rates of the released sulfate (r_{SO4}) are presented in Table 3. r_{SO4} was converted into corrosion current density (i_{SO4}), and the corresponding values are listed in Table 3. For conversion, we assumed that sulfate is produced according to following reaction:

$$FeS_2 + 8H_2O \rightarrow Fe^{2+} + 2SO_4^{2-} + 16H^+ + 14e^- \quad (2)$$

and current density is

$$i_{SO4} = 7 \times 10^{-4} \times F \times r_{SO4} \quad (3)$$

where r_{SO4} is the oxidation rate of pyrite and $F = 96{,}485$ C/mol. It can be seen that the corrosion current density measured by electrochemical method (i_{corr}) is higher than that determined from the released sulfate (i_{SO4}). Therefore, in acidic solutions, the monitoring of

Table 2 Electrochemical impedance parameters for pyrite in HCl solutions at pH 2.5 and containing different oxidants

Oxidant	R_s/Ω	R_{pl}/Ω	R_{ct}/Ω	C_{pl}/F	Q_{dl}/F (n_{dl})	W/DW	L_{py}/H	L_{pl}/H
Air-saturated solution	19.9	240.6	2.24×10^4	9.43×10^{-10}	2.17×10^{-4} (0.806)	–	–	–
$[H_2O_2] = 0.001$ M	15.4	249.5	1.54×10^4	8.74×10^{-10}	9.31×10^{-5} (0.687)	–	–	–
$[H_2O_2] = 0.1$ M	18.0	179.3	151.2	9.77×10^{-10}	2.96×10^{-4} (0.708)	–	2.44×10^{-5}	1.14×10^{-5}
$[Fe^{3+}]$=0.001 M	10.6	272.9	1.30×10^3	1.21×10^{-9}	4.65×10^{-5} (0.766)	381.8		
$[Fe^{3+}]$=0.01 M	7.5	90.5	105.1	1.97×10^{-9}	1.47×10^{-4} (0.812)	122.3		

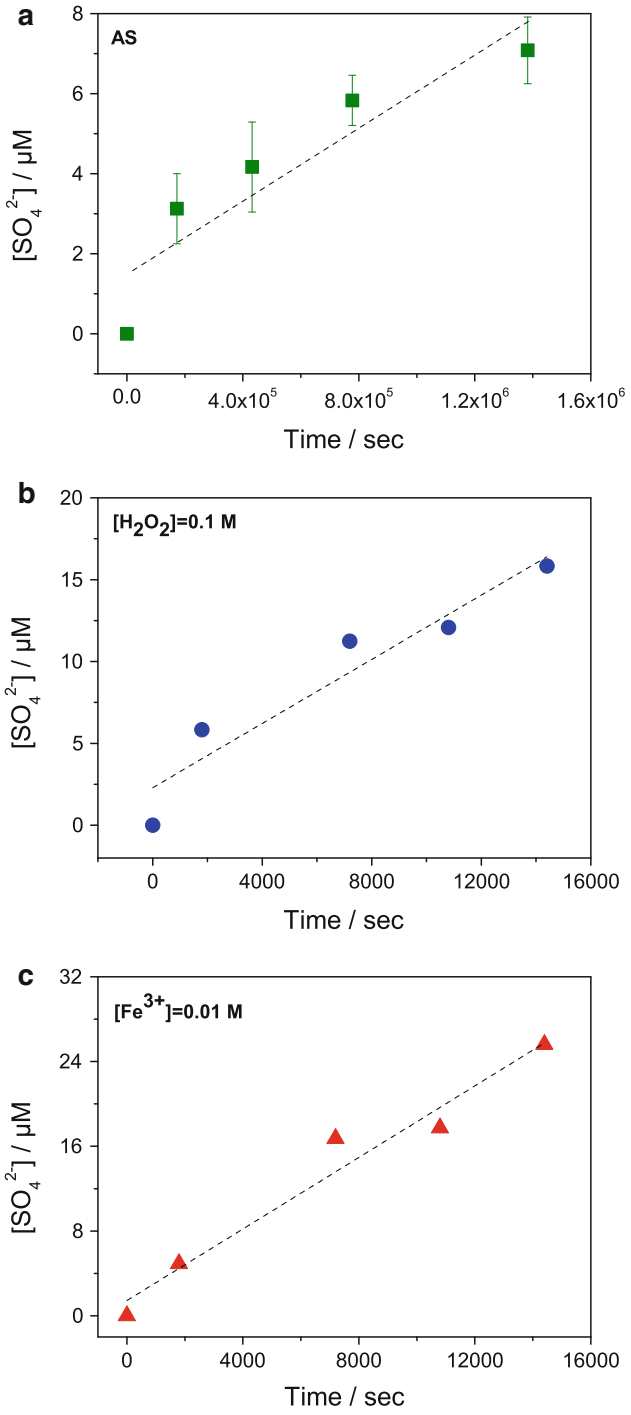

Fig. 5 Oxidative dissolution of pyrite in AS (**a**), H_2O_2, (**b**) and Fe^{3+} (**c**) solutions at 25 °C and pH 2.5. The *error bar* of each data point in graph (**a**) is the standard deviation

sulfate release will produce an underestimation of the rate of pyrite oxidation. The observed differences between i_{corr} and i_{SO4} suggest that either the mechanisms of the electrochemical oxidation of pyrite (oxidation of polarized electrode of pyrite) and chemical oxidation of pyrite particles are completely different or the overall mechanism of

Table 3 Oxidative dissolution rates (r_{SO4}), corresponding corrosion current densities (i_{SO4}) and i_{corr}:i_{SO4} ratios of pyrite in AS, H_2O_2, and Fe^{3+} solutions

Oxidant	Concentration/ M	r_{SO4}/ µmol s^{-1} m^{-2}	i_{SO4}/ µA cm^{-2}	i_{corr}:i_{SO4}
$O_{2(aq)}$	Saturated	2.53×10^{-4}	1.71×10^{-2}	104.1
$H_2O_{2(aq)}$	0.1	1.52×10^{-2}	1.03	138.8
$Fe^{3+}_{(aq)}$	0.01	9.35×10^{-2}	6.31	5.1

pyrite interaction with aqueous solutions is a result of both electrochemical and chemical mechanisms. We prefer to attribute the observed behavior to a mix of the two specific mechanisms. This is in agreement with the mechanism proposed by Wei and Osseo-Asare [9]. The mix of electrochemical and chemical mechanisms makes that only a fraction of pyrite sulfur to be oxidized to sulfate. As FTIR spectra indicate (Fig. 6), a series of other compounds with intermediate oxidation state of sulfur like polysulfide species, S^0 or $S_2O_3^{2-}$ are formed on mineral surface. The highest i_{corr}:i_{SO4} ratio was registered in the presence of $H_2O_{2(aq)}$; it decreases slightly for AS solution and decreases sharply when the oxidant is $Fe^{3+}_{(aq)}$. An additional reason for the high i_{corr}:i_{SO4} ratio obtained in the case of $H_2O_{2(aq)}$ is the decrease in $[H_2O_{2(aq)}]$ because of its decomposition by FeS_2 [12, 13]. The decrease in $[H_2O_{2(aq)}]$ will induce an underestimation of r_{SO4} and implicitly of i_{SO4}.

These findings are in good agreement with the previous studies that indicated a deficit in aqueous sulfur during oxidative dissolution of pyrite [2, 7]. The deficit of aqueous sulfur can be explained either by direct oxidation of pyrite to S^0 [25, 26]

$$FeS_2 + 1/2O_2 + 2H^+ \rightarrow Fe^{2+} + 2S^0 + H_2O \quad (4)$$

by $S_2O_3^{2-}$ disproportionation to S^0 and $S_4O_6^{2-}$ [7]

$$FeS_2 + 3/2O_2 \rightarrow Fe^{2+} + S_2O_3^{2-} \quad (5)$$

$$S_2O_3^{2-} + 6/5H^+ \rightarrow 2/5S_4O_6^{2-} + 2/5S^0 + 3/5H_2O \quad (6)$$

or both. i_{corr}:i_{SO4} values registered in the presence of H_2O_2 and AS solutions are too large to be explained only by the disproportionation of $S_2O_3^{2-}$. Most probably, they are the result of direct oxidation of pyrite to S^0 [reaction (4)]. The reactions (5) and (6) can be taken into account in the case of $Fe^{3+}_{(aq)}$.

3.4 FTIR measurements

The FTIR spectra of the initial and reacted pyrite samples are presented in Fig. 6. From this figure, one observes that the spectrum of initial sample has fewer and weaker peaks, indicating that the degree of oxidation of the initial pyrite is

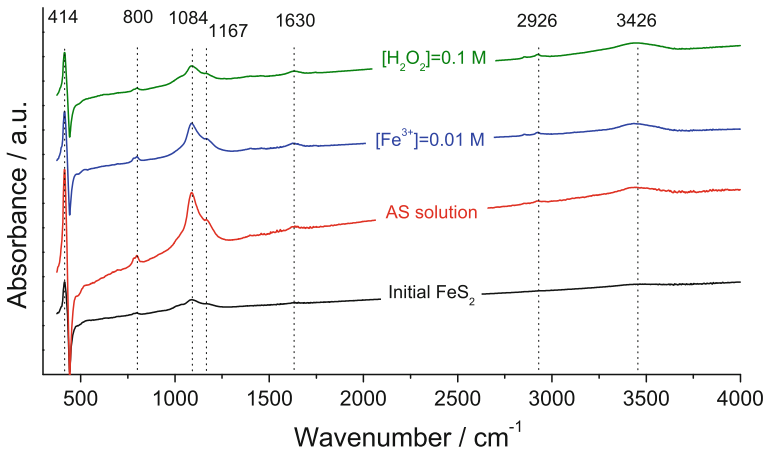

Fig. 6 FTIR spectra for the initial and reacted pyrite samples in AS, H_2O_2, and Fe^{3+} solutions at pH 2.5

lower than that of the reacted samples. All the peaks present in Fig. 6 can be attributed to pyrite (disulfide) and its specific reaction products of oxidation. The signal registered at 414 cm^{-1} can be assigned to S–S stretching vibrations (polysulfide, elemental sulfur but also disulfide) [17–20]. The peak observed at 800 cm^{-1} is due to Fe–O–H bending vibrations of goethite and $Fe(OH)_3$ [17, 18]. The band observed in the 950–1,300 cm^{-1} region indicates the presence of oxysulfur species [17–20] like HSO_4^- (1,167 cm^{-1}) and $S_2O_3^{2-}$ (1,090 cm^{-1}). The peak at 1,640 cm^{-1} can be assigned to H–O–H deformations [18]. The peak at 2,926 cm^{-1} and band centered to 3,426 cm^{-1} can be assigned to stretching modes in goethite and amorphous $Fe(OH)_3$ [17, 18].

4 Conclusions

The pyrite oxidative dissolution in AS, H_2O_2, and Fe^{3+} solutions (pH 2.5) was studied by electrochemical and aqueous batch experiments. The obtained results have indicated different mechanisms of the oxidation of pyrite in the presence of the three oxidants. The polarization measurements have indicated that during anodic oxidation of pyrite in the presence of 0.01 M Fe^{3+} solution on mineral surface is developed a passive film, most probably formed by elemental sulfur. No similar behavior was observed for the other solutions. EIS measurements have indicated that in AS and H_2O_2 solutions, the charge transfer is the rate determining step of pyrite oxidative dissolution. In the presence of $Fe^{3+}_{(aq)}$, both the charge transfer process and mass transfer caused by the diffusion of oxidant or reaction products across the interface of electrode control the mineral oxidative dissolution. It was found that rates of oxidative dissolution measured by electrochemical methods are higher than the rates determined by aqueous bath experiments. The observed differences indicate that the mechanisms of polarized electrode oxidation are different by the mechanisms of pyrite oxidation under open circuit conditions, when a mix of electrochemical and chemical processes occurs.

Acknowledgments This work was partially supported by the strategic grant POSDRU/CPP107/DMI1.5/S/78421, Project ID 78421 (2010), co-financed by the European Social Fund-Investing in People, within the Sectorial Operational Programme Human Resources Development 2007–2013.

References

1. McKibben MA, Barnes HL (1986) Oxidation of pyrite in low temperature acidic solutions: rate laws and surface textures. Geochim Cosmochim Acta 50:1509–1520
2. Peiffer S, Stubert I (1999) The oxidation of pyrite at pH 7 in the presence of reducing and nonreducing Fe(III)-chelators. Geochim Cosmochim Acta 63:3171–3182
3. Lin HK, Say WC (1999) Study of pyrite oxidation by cyclic voltammetric, impedance spectroscopic and potential step techniques. J Appl Electrochem 29:987–994
4. Flatt JR, Woods R (1995) A voltammetric investigation of the oxidation of pyrite in nitric-acid solutions—relation to treatment of refractory gold ores. J Appl Electrochem 9:852–856
5. Giannetti BF, Almeida CMVB, Bonilla SH (2006) Electrochemical kinetic study of surface layer growth on natural pyrite in acid. Colloids Surf A: Physicochem Eng Aspects 272:130–138
6. Liu R, Wolfe AL, Dzombak DA, Horwitz CP, Stewart BW, Capo RC (2008) Electrochemical study of hydrothermal and sedimentary pyrite dissolution. Appl Geochem 23:2724–2734
7. Descostes M, Vitorge P, Beaucaire C (2004) Pyrite dissolution in acidic media. Geochim Cosmochim Acta 6:4559–4569
8. Sasaki K, Tsunekawa M, Ohtsuka T, Konno H (1995) Confirmation of a sulfur-rich layer on pyrite after oxidative dissolution by Fe(III) ions around pH 2. Geochim Cosmochim Acta 59:3155–3158
9. Wei D, Osseo-Asare K (1997) Semiconductor electrochemistry of particulate pyrite. Mechanism and products of dissolution. J Electrochem Soc 144:546–553
10. Luther GW III (1997) Comment on Confirmation of a sulfur-rich layer on pyrite after oxidative dissolution by Fe(III) ions around pH 2 by K. Sasaki, M. Tsunekawa, T. Ohtsuka, and H. Konno. Geochim Cosmochim Acta 61:3269–3271

11. Williamson MA, Rimstidt JD (1994) The kinetics and electrochemical rate-determining step of aqueous pyrite oxidation. Geochim Cosmochim Acta 58:5443–5454
12. Chirita P (2007) A kinetic study of hydrogen peroxide decomposition in presence of pyrite. Chem Biochem Eng Q 21:257–264
13. Chirita P (2009) Hydrogen peroxide decomposition by pyrite in the presence of Fe(III)-ligands. Chem Biochem Eng Q 23:259–265
14. Liu J, Aruguete DM, Jinschek JR, Rimstidt JD, Hochella MF Jr (2008) The non-oxidative dissolution of galena nanocrystals: insights into mineral dissolution rates as a function of grain size, shape, and aggregation state. Geochim Cosmochim Acta 72:5984–5996
15. Manescu S, Cucu M, Diaconescu ML (1994) Chimia sanitara a mediului. Editura Medicala, Bucuresti
16. Caldeira CL, Ciminelli VST, Osseo-Asare K (2010) The role of carbonate ions in pyrite oxidation in aqueous systems. Geochim Cosmochim Acta 74:1777–1789
17. Mikhlin YuL, Kuklinskiy AV, Pavlenko NI, Varnek VA, Asanov IP, Okotrub AV, Selyutin GE, Solovyev LA (2002) Spectroscopic and XRD studies of the air degradation of acid-reacted pyrrhotites. Geochim Cosmochim Acta 66:4057–4067
18. Chirita P, Descostes M, Schlegel ML (2008) Oxidation of FeS by oxygen-bearing acidic solutions. J Colloid Interface Sci 321:84–95
19. Weerasooriya R, Indraratne SP, Nanayakkara N, Jayarathne L, Dissanayake CB, Walalawela N, Bandara A (2012) Probing pyrite–carbofuran interactions with ζ potential and IR spectroscopic measurements. Colloids Surf A: Physicochem Eng Aspects 396: 219–223
20. Weerasooriya R, Makehelwala M, Bandara A (2010) Probing reactivity sites on pyrite-oxidative interactions with 4-chlorophenol. Colloids Surf A: Physicochem Eng Aspects 367:65–69
21. Velasquez P, Leinen D, Pascual J, Ramos-Barrado JR, Grez P, Gomez H, Schrebler R, Del Rio R, Cordova R (2005) A Chemical, morphological, and electrochemical (XPS, SEM/EDX, CV, and EIS) analysis of electrochemically modified electrode surfaces of natural chalcopyrite ($CuFeS_2$) and pyrite (FeS_2) in alkaline solutions. J Phys Chem B 109:4977–4988
22. Liu Y, Dang Z, Lu G, Wu P, Feng C, Yi X (2011) Utilization of electrochemical impedance spectroscopy for monitoring pyrite oxidation in the presence and absence of *Acidithiobacillus ferrooxidans*. Min Eng 24:833–838
23. Lehner S, Ciobanu M, Savage K, Cliffel DE (2008) Electrochemical impedance spectroscopy of synthetic pyrite doped with As, Co and Ni. J Electrochem Soc 155:P61–P70
24. Ghahremaninezhad A, Asselin E, Dixon DG (2010) Electrochemical evaluation of the surface of chalcopyrite during dissolution in sulfuric acid solution. Electrochim Acta 55:5041–5056
25. Tao DP, Richardson PE, Luttrell GH, Yoon RH (2003) Electrochemical studies of pyrite oxidation and reduction using freshly-fractured electrodes and rotating ring-disc electrodes. Electrochim Acta 48:3615–3623
26. Safarzadeh MS, Li J, Moats MS, Miller JD (2012) The stability of selected sulfide minerals in sulfuric acid and acidic thiocyanate solutions. Electrochim Acta 78:133–138